ORIGINAL ARTICLE

Cancer Science WILEY

EZH2 suppresses ferroptosis in hepatocellular carcinoma and reduces sorafenib sensitivity through epigenetic regulation of TFR2

Yongwei Lai[1] | Xu Han[1] | Bo Xie[1] | Yan Xu[1] | Zhengyi Yang[1] | Didi Wang[1] |
Wei Li[2] | Yaohong Xie[1] | Wenqi Song[1] | Xiaohong Zhang[3] | Jia Qi Xia[1] |
Pengxia Zhang[1]

[1]Key Laboratory of Microecology-Immune Regulatory Network and Related Diseases School of Basic Medicine, Jiamusi University, Jiamusi, China

[2]School of Clinical Medicine, Jiamusi University, Jiamusi, China

[3]Department of Basic Medicine, Jiangsu Vocational College of Medicine, Yancheng, China

Correspondence
Pengxia Zhang and Jia Qi Xia, No. 258 XueFu Street Xiangyang district Jiamusi, Heilongjiang 154000, China.
Email: pengxiaz@jmsu.edu.cn and jiaqixia@whu.edu.cn

Abstract

Enhancing sensitivity to sorafenib can significantly extend the duration of resistance to it, offering substantial benefits for treating patients with hepatocellular carcinoma (HCC). However, the role of ferroptosis in influencing sorafenib sensitivity within HCC remains pivotal. The enhancer of zeste homolog 2 (EZH2) plays a significant role in promoting malignant progression in HCC, yet the relationship between ferroptosis, sorafenib sensitivity, and EZH2 is not entirely clear. Bioinformatic analysis indicates elevated EZH2 expression in HCC, predicting an unfavorable prognosis. Overexpressing EZH2 can drive HCC cell proliferation while simultaneously reducing ferroptosis. Further analysis reveals that EZH2 amplifies the modification of H3K27 me3, thereby influencing TFR2 expression. This results in decreased RNA polymerase II binding within the TFR2 promoter region, leading to reduced TFR2 expression. Knocking down EZH2 amplifies sorafenib sensitivity in HCC cells. In sorafenib-resistant HepG2(HepG2-SR) cells, the expression of EZH2 is increased. Moreover, combining tazemetostat—an EZH2 inhibitor—with sorafenib demonstrates significant synergistic ferroptosis-promoting effects in HepG2-SR cells. In conclusion, our study illustrates how EZH2 epigenetically regulates TFR2 expression through H3K27 me3, thereby suppressing ferroptosis. The combination of the tazemetostat with sorafenib exhibits superior synergistic effects in anticancer therapy and sensitizes the HepG2-SR cells to sorafenib, shedding new light on delaying and ameliorating sorafenib resistance.

KEYWORDS
EZH2, ferroptosis, hepatocellular carcinoma, sorafenib, TFR2

---

1 | INTRODUCTION

Hepatocellular carcinoma (HCC) is a common cancer with a low survival rate for most patients.[1] Sorafenib, an FDA-approved first-line systemic therapy, increases median overall survival for advanced-stage HCC patients.[2] This drug functions as a multi-target kinase inhibitor, inhibiting growth factor receptors such as vascular endothelial growth factor receptor and platelet-derived growth factor receptor.[3] Regrettably, only approximately 30% of patients experience positive outcomes from sorafenib treatment, with many developing resistance within 6 months.[4] Overcoming sorafenib resistance poses a significant challenge, necessitating rational combination therapies to enhance its effectiveness.

Studies indicate that sorafenib inhibits SLC7A11, leading to the accumulation of ROS and the induction of ferroptosis.[5] Sorafenib can induce ferroptosis in HCC cells by depleting GSH levels or increasing mitochondrial ROS production, independently or reliant on the retinoblastoma protein.[6] Recent research underscores that inducing intracellular ferroptosis significantly enhances the efficacy of sorafenib, particularly in human HCC cases where chemotherapy resistance to sorafenib has already been reported.[7]

EZH2, a member of the polycomb repressive complex 2 (PRC2), is recognized for its role in catalyzing trimethylation of lysine 27 on histone 3 (H3K27 me3), thereby inducing transcriptional repression of target genes.[8,9] Numerous studies have investigated the aberrant expression of PRC2 and/or EZH2 across a wide spectrum of human cancers.[10] Cancer cells exhibit a higher demand for iron to support their proliferation, rendering them more susceptible to ferroptosis, a process leading to cancer cell death.[11-13] Various epigenetic mechanisms, including DNA methylation, histone modification, and post-transcriptional modification, have been demonstrated to regulate iron homeostasis.[14] Studies suggest a link between HCC resistance to sorafenib and iron metabolism and ferroptosis, but the exact mechanism behind this is unclear.

In our present study, we aimed to elucidate the involvement of EZH2 in sorafenib resistance and ferroptosis. We found that EZH2 suppresses TFR2 expression through epigenetic regulation, elevates the H3K27 me3 levels in the TFR2 promoter region, diminishes RNA polymerase II recruitment, lowers intracellular iron levels, impedes the Fenton reaction, mitigates ferroptosis in HCC, and reduces sorafenib-induced ferroptosis. Combining the EZH2 inhibitor tazemetostat with sorafenib enhanced the efficacy against HCC, ameliorating the development of sorafenib resistance. This combined approach presents a potential novel strategy for increasing sorafenib sensitiveness in HCC patients.

2 | MATERIALS AND METHODS

2.1 | Clinical specimens of patients

Eight HCC patients had surgery at the Affiliated Hospital of Jiamusi University. Tumor and adjacent tissues were analyzed as histopathological sections. The study was approved by the Ethical Review Committee of Jiamusi University, and all patients gave informed consent.

2.2 | Antibodies and reagents

The antibodies of SLC7A11 (Cat.AF7992) and GPX4 (Cat. AF7020) were purchased form Beyotime; EZH2 (Cat.21800–1), NRF2 (Cat.16396–1), HRP-conjugated β-actin (Cat.HRP-60008), H3K27me3 (Cat.61018), and H3K27ac (Cat.39 085) were obtained from Proteintech; and TFR2 (Cat. A9845) was purchased form ABClonal. Sorafenib (Cat.S1040) and tazemetostat (Cat.S7128) were purchased form Selleck. Z-VAD-FMK (Cat.HY16658), necrosulfonamide (Cat.HY100573), ferrostatin-1 (Cat.HY-100579), and bafilomycin A1 (Cat.HU-100558) were purchased form MedChemExpress.

2.3 | Bioinformatics analysis

TIMER2 (TIMER2; http://timer.cistrome.org) and TCGA (TCGA; https://portal.gdc.cancer.gov/) database analysis EZH2 expression variations across various tumors and normal tissues. Microarray data (GSE102083, GSE6764, GSE45436, GSE39791, GSE64041) from the Gene Expression Omnibus (GEO) database (https://www.ncbi.nlm.nih.gov/geo/) were utilized to examine the differential expression of EZH2 and TFR2 between normal and HCC tissues. Additionally, the GEPIA database (http://gepia.cancer-pku.cn/) was employed for EZH2 expression analysis and patient prognosis evaluation. Iron metabolism-related genes were sourced from the GeneCards database (https://www.genecards.org/), while ferroptosis driver genes were obtained from the FerrDb database (http://www.zhounan.org/ferrdb/current/).

2.4 | Cell culture and transfection

Hepatocellular carcinoma cell lines HepG2 and Huh-7 were obtained from the ATCC and cultured in DMEM with 10% FBS, penicillin, and streptomycin at 5% CO_2 and 37°C. siRNAs were transfected using the riboFECT™ CP transfection kit, and EZH2 plasmid was transfected using Lipo8000™ transfection reagent. Target sequences of siRNA are listed in Table S1.

2.5 | Real-time quantitative reverse-transcription polymerase chain reaction (qRT-PCR)

RNA was extracted with the Total RNA extraction kit (Cat.SM132, Sevenbio), and cDNA was synthesized using the First Strand cDNA synthesis kit (Cat.D7178. Beyotime). qRT-PCR was performed using 2×SYBR qPCR Master Mix (Cat.ZF503, Zomanbio) and an ABI7300 instrument (Applied Biosystems) with the $2^{-\Delta\Delta Ct}$ method

for relative gene expression calculation. Primer sequences are listed in Table S2.

2.6 | Chromatin immunoprecipitation assay

Cells were washed, crosslinked, and lysed to yield chromatin fragments. Input samples were reserved, while the remaining chromatin was incubated with antibody. Immunocomplexes were washed, eluted, and analyzed by PCR. Primer details are listed in Table S3.

2.7 | Western blot

Total proteins were extracted using RIPA buffer with a protease inhibitor, separated using SDS-PAGE, transferred to PVDF membranes, blocked, and incubated with primary and secondary antibodies before imaging with a chemiluminescence imager (E-blot).

2.8 | Histopathological analysis

The tissue was preserved, embedded, sliced, treated with xylene, and dehydrated for IHC analysis. Samples were incubated with primary antibodies, secondary antibodies, diaminobenzidine (DAB) staining, and restaining. The mixture was sealed, imaged, and analyzed using ImageJ software for positive immunostaining and cumulative light intensity.

2.9 | Colony formation assays

Single-cell suspension cells were cultured in six-well plates for 24 h, replaced every 72 h, and cultivated for 2 weeks. Colonies were fixed, stained, washed three times, and analyzed using imaging system.

2.10 | Cell viability assay

Cells were plated in 96-well plates at 5000 cells per well after transfection with EZH2 plasmid or EZH2 siRNA. They were then treated with different concentrations of drugs for 24–72 h. Cell viability was assessed using CCK-8 assay.

2.11 | Assays of iron, MDA, and GSH content

The Iron Assay Kit (Cat.b83366, Abcam) was utilized following the manufacturer's guidelines to determine the total iron content. MDA concentration assay kit (Cat. S0131, Beyotime) and GSH concentration assay kit (Cat.S0053, Beyotime) was determined the cell extract following the manufacturer's instructions.

2.12 | Reactive oxygen species and mitochondrial membrane potential detection assay

DCFH-DA (Cat.S0033, Beyotime) or JC-1 (Cat.HY-K0601, MedChemExpress) was added and incubated for 20 min at 37°C in an incubator. The cells were inverted and mixed every 3–5 min, washed three times with serum-free cell culture medium, and observed using a fluorescence microscope (APX100, Olympus).

2.13 | In vivo tumorigenesis and drug treatment

Approval from the Ethics Committee of Jiamusi University was obtained for the animal study. Each 6-week-old male mouse was injected with 1×10^7 H22 cells, and tumor volumes were monitored every 3 days. Mice with tumors of 150–250 mm^3 were divided into four groups: NC (saline), sorafenib (10 mg/kg/day), tazemetostat (125 mg/kg/day), and combination treatment groups (10 mg/kg/day sorafenib +125 mg/kg/day tazemetostat). After 3 weeks, mice were euthanized, and the tumors were resected and weighed. A portion of the tumor tissue was preserved in formalin solution.

2.14 | Transmission electron microscope (TEM)

Centrifuged cell clumps were fixed with 2.5% glutaraldehyde overnight at 4°C, dehydrated in graded ethanol series, and embedded in epoxy resin. Thin sections were imaged by TEM (JEM-1400, JEOL).

2.15 | Statistical analysis

All statistical analyses were conducted using GraphPad Prism 8.0 software (GraphPad Software) utilizing either one-way analysis of variance or Student's t-test. Data are presented as mean ± SD. p-values of less than 0.05 indicated statistical significance (*$p < 0.05$; **$p < 0.01$; ***$p < 0.001$).

3 | RESULTS

3.1 | EZH2 expression is upregulated in HCC and predicts an unfavorable prognosis

Exploring EZH2 expression across various malignancies utilized the TIMER2 dataset. The majority of tumors, including HCC, exhibited increased EZH2 expression (Figure S1A). EZH2 expression in HCC was significantly higher in HCC tissues than in normal tissues in TCGA database (Figure 1A,B). Higher EZH2 expression in tumor tissues than in normal tissues was consistent across five datasets from the GEO database (Figure S1B). Elevated EZH2 expression showed a significant association with lymph node metastasis
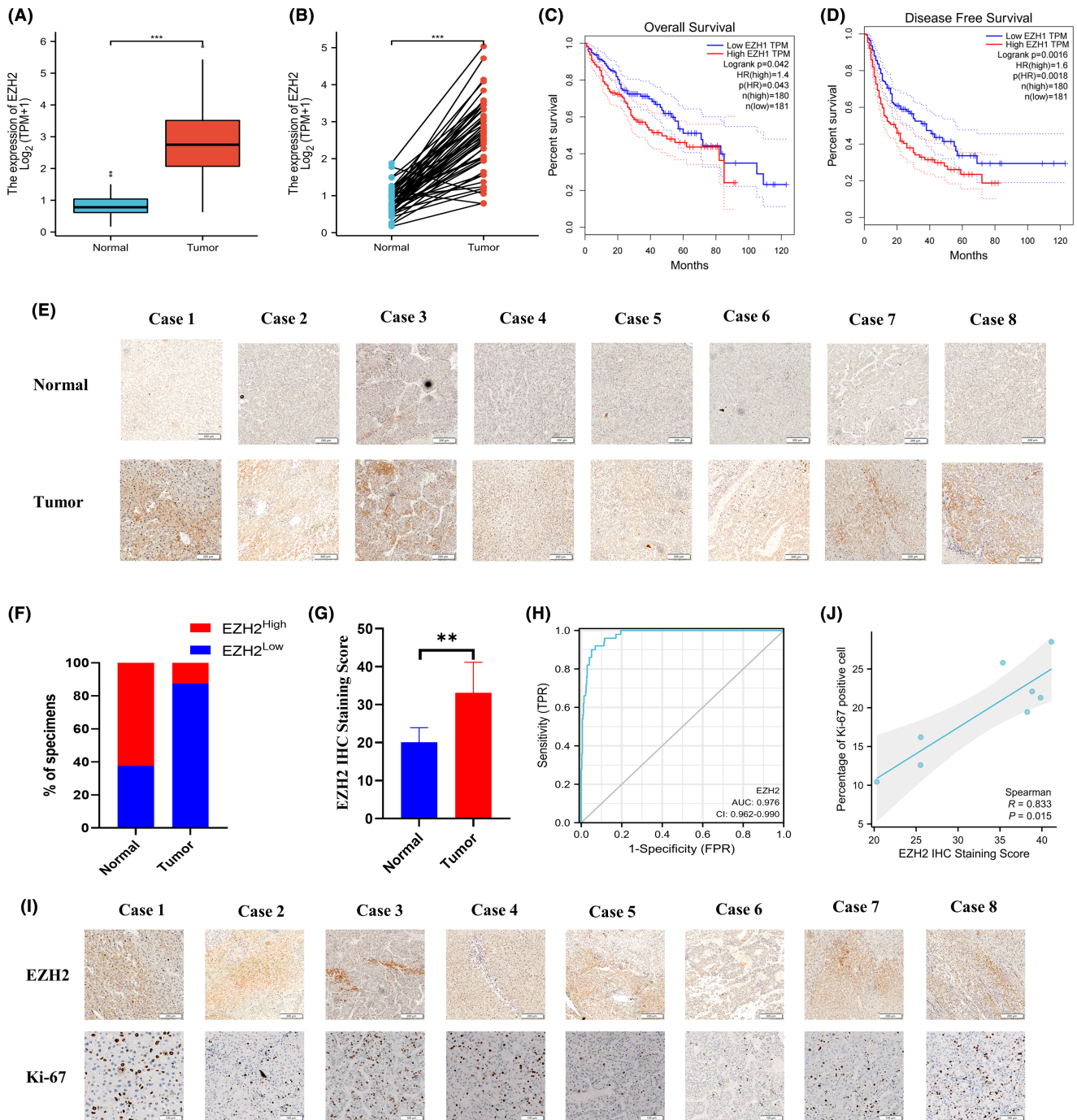
FIGURE 1 EZH2 expression is upregulated in hepatocellular carcinoma and predicts an unfavorable prognosis. (A) Expression of EZH2 in unpaired ($n = 371$) and (B) paired hepatocellular carcinoma (HCC) tissue samples from TCGA database ($n = 50$). (C, D) Kaplan–Meier survival curve analysis of the EZH2 high-expression group versus low-expression group of OS and DFS ($n = 371$). (E) EZH2 expression in eight HCC patients. (F) Percentage of high expression of EZH2 in eight HCC patients. (G) Expression of EZH2 in eight tumor and normal tissues. (H) Receiver-operating characteristic curve (ROC) analysis of EZH2 in HCC patients ($n = 371$). (I) Ki-76 expression in HCC tissues from patients ($n = 8$). (J) Correlation between Ki-67 and EZH2 expression ($n = 8$). **$p < 0.01$; ***$p < 0.001$.

(Figure S1C). Moreover, EZH2 expression levels correlated with cancer stage and tumor grade, increasing with higher stages and grades (Figure S1D,E). Notably, increased EZH2 expression in HCC patients was linked to shorter OS and DFS (Figure 1C,D). IHC analysis of eight pairs of HCC tissues further confirmed elevated EZH2 expression in

HCC (Figure 1E–G). ROC curve exhibited a high area under the curve of 0.976, underscoring EZH2's potential as a diagnostic marker for HCC (Figure 1H). Additionally, a positive correlation between EZH2 expression and Ki-67 was observed in the GEPIA database and further confirmed using IHC in clinical samples (Figure S1F, Figure 1I,J).
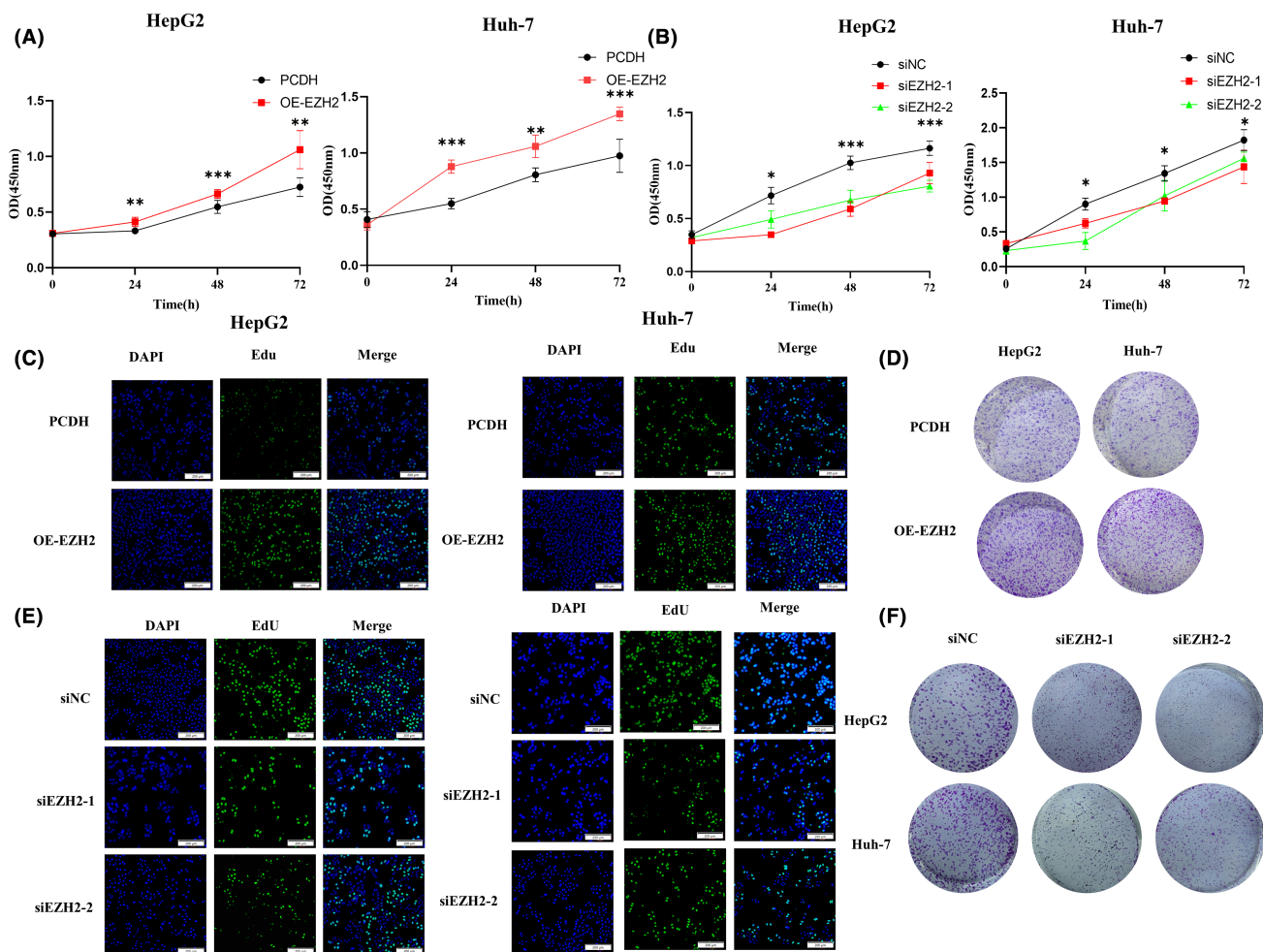
FIGURE 2 EZH2 promotes hepatocellular carcinoma cell proliferation. (A, B) EZH2 overexpression or knockdown detected by cell viability assay using CCK-8 ($n = 6$). (C, E) EdU staining detected cell proliferation after EZH2 overexpression or knockdown ($n = 3$). Scale bar $= 200\,\mu m$. (D, F) Colony formation assay indicated EZH2 overexpression or knockdown ($n = 3$). $^*p < 0.05$; $^{**}p < 0.01$; $^{***}p < 0.001$.

These collective findings highlight the upregulation of EZH2 in HCC and its potential as a valuable predictive biomarker.

3.2 | EZH2 promotes HCC cell proliferation

EZH2 showed high expression levels in HCC patients, correlating with a poor prognosis, prompting an investigation into its role in HCC. CCK-8 results demonstrated that elevated EZH2 levels promoted the proliferation of HepG2 and Huh-7 cells (Figure 2A). Conversely, the reduction of EZH2 inhibited cell proliferation (Figure 2B). Colony formation assay and EdU staining were conducted to assess proliferation and clonogenic potential. Significant increase was observed in the count of EdU-positive cells and the number of clones upon EZH2 overexpression (Figure 2C,D, Figure S2A,B). Conversely, the count of EdU-positive cells and clone number decreased following EZH2 knockdown (Figure 2E,F, Figure S2C,D). Collectively, these results suggest that EZH2 promotes cell proliferation and contributes to the malignant progression of HCC.

3.3 | EZH2 inhibits HCC cell ferroptosis

EZH2 in HepG2 cells was knocked down, and various inhibitors **were** added: bafilomycin A1 (an autophagy inhibitor), Z-VAD-FMK (an apoptosis inhibitor), necrosulfonamide (a necrosis inhibitor), and ferrostatin-1 (a ferroptosis inhibitor) for treatment. The rescue of cell viability inhibition induced by siEZH2–1 was observed with bafilomycin A1 and ferrostatin-1, while siEZH2–2 was only rescued by ferrostatin-1 (Figure 3A). This outcome suggests that EZH2 might be involved in inhibiting apoptosis or ferroptosis. To test this hypothesis, EZH2 was overexpressed in HepG2 cells and subsequently treated with the erastin. Results showed that EZH2 overexpression countered the decrease in cell viability induced by erastin (Figure 3B). The PCR analysis of cells overexpressing EZH2 in HepG2 and Huh-7 cells revealed elevated mRNA levels of SLC7A11 and NRF2, but no significant effect on GPX4 mRNA levels (Figure 3C). These findings were consistent with Western blot results (Figure 3D, Figure S3A). Conversely, silencing EZH2 resulted in unchanged GPX4 and downregulated NRF2 and SLC7A11 in mRNA (Figure 3E) and protein level (Figure 3F, Figure S3B). Overexpressing EZH2 in HepG2 and Huh-7
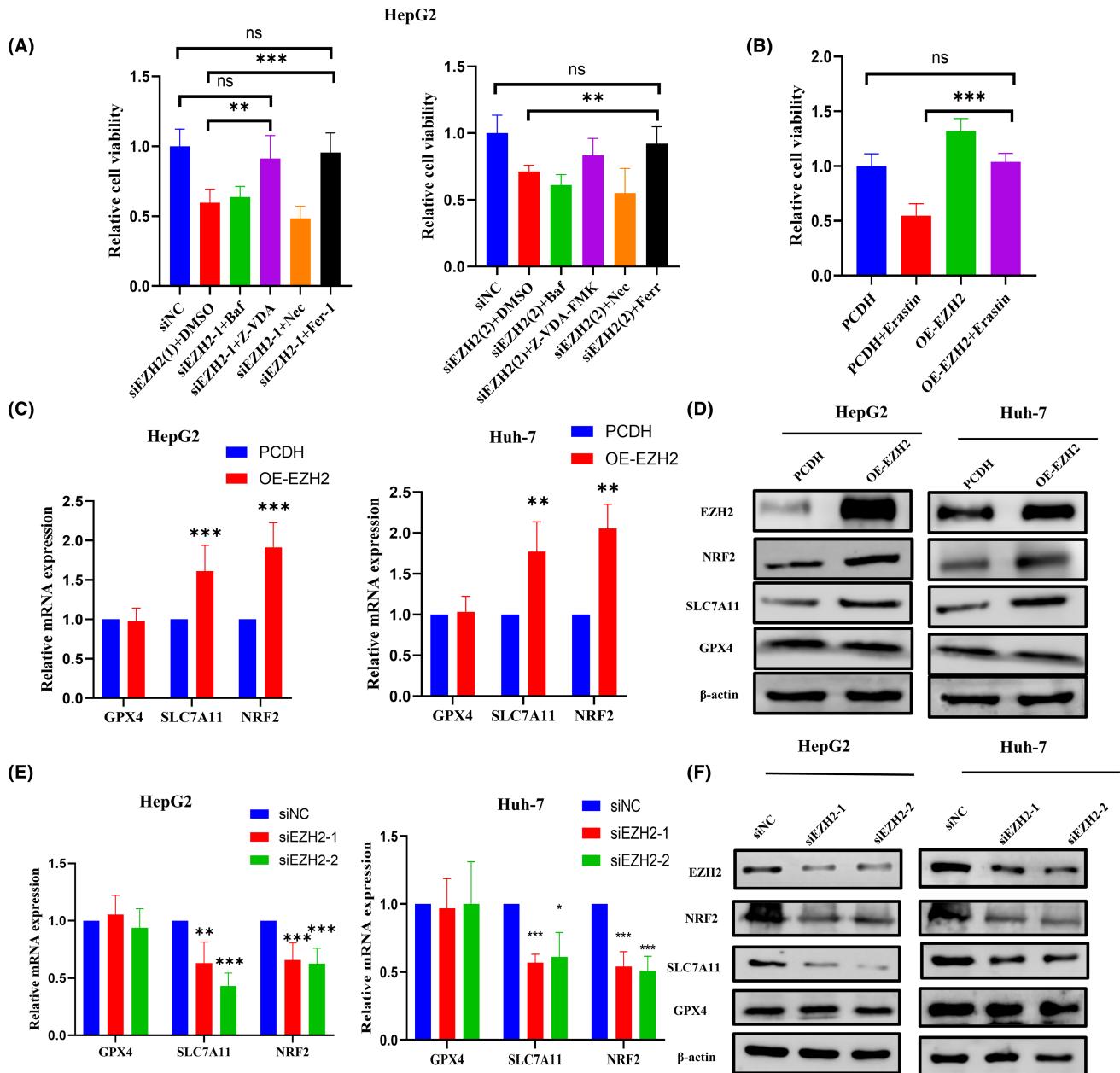
FIGURE 3 EZH2 inhibits hepatocellular carcinoma cell ferroptosis. (A) Cell viability was determined using CCK-8 assays in HepG2 cells with EZH2 knockdown that were treated with different cell death inhibitors ($n=3$). (B) Cell viability was determined using CCK-8 assays in HepG2 cells that had EZH2 overexpression and were treated with erastin ($n=3$). (C, D) Detection of the ferroptosis-related genes with EZH2 overexpression using PCR or Western blot ($n=3$). (E, F) Detection of the ferroptosis-related genes with EZH2 overexpression using PCR or Western blot ($n=3$). $*p<0.05$; $**p<0.01$; $***p<0.001$.

cells was found to decrease intracellular iron levels (Figure 4A). Subsequent experiments involved the addition of 100 μM FeSO$_4$ after EZH2 overexpression, revealing a reduction in iron levels compared with the FeSO$_4$-only group (Figure 4B). Additionally, EZH2 overexpression was linked to reduced intracellular levels of ROS and MDA levels and increased GSH/GSSH ratio (Figure 4C–E), while EZH2 knockdown exhibited contrasting results (Figure 4F,G). These data collectively suggest that EZH2 overexpression in HCC could mitigate cell ferroptosis.

3.4 | EZH2 inhibits sorafenib-induced ferroptosis

Moreover, the GSH/GSSG ratio increased and MDA production was reduced upon EZH2 overexpression and sorafenib treatment in HepG2 cells. Chemotherapy drugs are essential for extending patient survival. High EZH2 expression was found to decrease sensitivity to various chemotherapeutic drugs, including sorafenib (Figure 5A). The overexpression of EZH2 resulted in decreased sensitivity of HepG2 and Huh-7 cells to sorafenib, thereby enhancing cell proliferation and
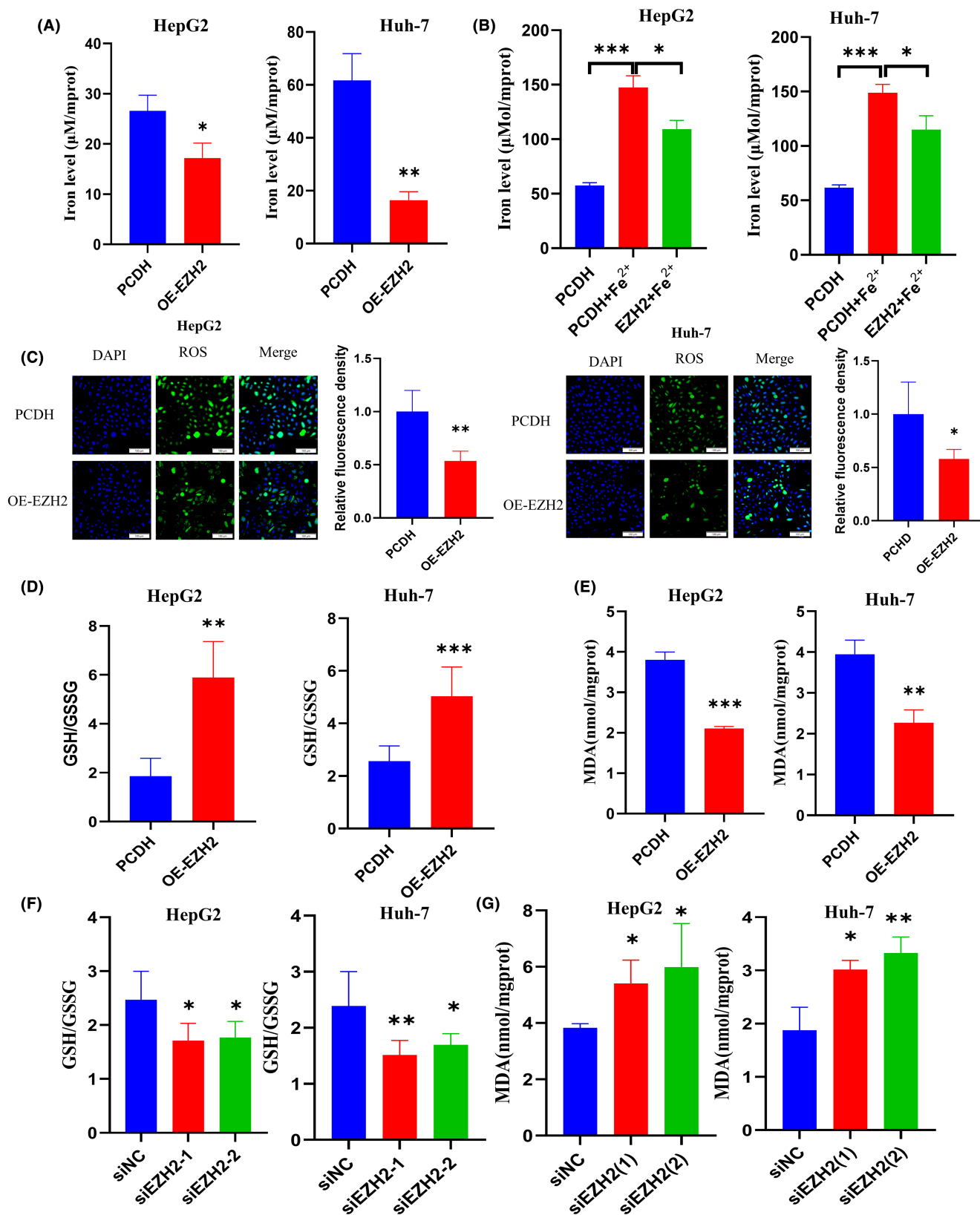
FIGURE 4 Effect of EZH2 on antioxidant capacity. (A) Intracellular iron concentrations of HepG2 and Huh-7 cells that had EHZ2 overexpression ($n = 3$). (B) Detection of iron concentration in cells after overexpression of EZH2 using $FeSO_4$ treatment ($n = 3$). (C, D) Detection of reactive oxygen species (ROS) levels in EZH2 overexpression or knockdown of HepG2 cells ($n = 3$). Scale bar = 100 μm. (E, F) Intracellular GSH levels were detected in EZH2 overexpression and knockdown of HepG2 and Huh-7 cells ($n = 3$). (G). Intracellular malondialdehyde (MDA) concentrations of HepG2 and Huh-7 cells with EHZ2 overexpression and knockdown ($n = 3$). *$p < 0.05$; **$p < 0.01$; ***$p < 0.001$.

clonogenic potential (Figure 5B,C, Figure S3C). Additionally, EdU staining demonstrated a significantly higher number of EdU-positive cells in HepG2 cells overexpressing EZH2 and incubated with sorafenib compared with the sorafenib-only group (Figure 5D, Figure S3D). Given sorafenib's role as a ferroptosis inducer, it was hypothesized that EZH2 reduces sensitivity by impeding sorafenib-induced ferroptosis. Cells with EZH2 overexpression followed by sorafenib administration exhibited lower ROS levels compared with the sorafenib-only group (Figure 5E, Figure S3E). The transfer vector or EZH2 plasmid were introduced into HepG2 cells and subsequently treated with sorafenib. Upon comparison with the vector group, the EZH2 plasmid group exhibited an increase in the GSH/GSSG ratio and a decrease in MDA levels (Figure 5F,G). EZH2 overexpression and sorafenib incubation increased the fluorescence intensity of JC-1 aggregates and decreased JC-1 monomers' fluorescence intensity (Figure 5H). We further examined mitochondrial morphology using TEM and found that the mitochondria in sorafenib-treated HepG2 were ruptured, with distorted cristae and reduced cristae density. In contrast, EZH2 prevented such mitochondrial damage (Figure 5I). These results highlight that EZH2 diminishes the sensitivity of HCC cells to sorafenib by impeding sorafenib-induced ferroptosis.

3.5 | EZH2 represses the expression of TFR2 through histone H3K27me3 modification

EZH2 inhibits gene expression by trimethylating histone H3K27. Therefore, we screened genes negatively correlated with EZH2 using the TCGA database. EZH2 can suppress ferroptosis by modulating iron levels. Consequently, we screened genes associated with iron metabolism using the GeneCards database and ferroptosis driver genes through the FerrDB website. The Venn diagram revealed overlap genes: TFR2, SLC25A28, ACO1, SLC39A14, and IL6 (Figure 6A). Among these, TFR2 showed the most negative correlation with EZH2, making it a potential candidate gene (Figure 6B and Figure S4A). The analysis of data from the TCGA and GEO databases revealed a significantly lower expression of TFR2 in HCC tissues compared to normal tissues (Figure 6C and Figure S4B). IHC analysis of eight cases revealed reduced TFR2 levels in tumor tissues compared with normal tissues (Figure 6D and Figure S4C). A significant negative correlation between TFR2 and KI-67 was evident in the GEPIA database (Figure S4D). IHC examination of TFR2 expression in eight clinical pathological tissue samples confirmed a negative correlation between TFR2 and KI-67 expression (Figure S4E,F).

These results collectively indicate downregulated TFR2 expression in HCC, implicating its involvement in HCC progression.

The TFR2 mRNA levels were significantly reduced by overexpression of EZH2 (Figure 6E), while at the protein level, overexpression of EZH2 increased H3K27ME3 and decreased TFR2 (Figure 6F, Figure S4G). Knockdown of EZH2 had the opposite effect (Figure 6G,H, Figure S4H). Chromatin immunoprecipitation was employed to examine the extent of trimethylation and acetylation of histone H3K27 within the promoter region of TFR2 by EZH2. The findings indicated that the overexpression of EZH2 led to an elevation in the trimethylation level of H3K27 and a decrease in the acetylation level within the promoter region of TFR2 in both HepG2 cells and Huh-7 cells (Figure 6I,J). Furthermore, the recruitment of RNA polymerase II at the promoter region of TFR2 was diminished subsequent to the overexpression of EZH2 (Figure 6K). Based on the aforementioned data, it can be concluded that EZH2 enhances the H3K27 trimethylation level within the promoter region of TFR2, which affects the binding of RNA polymerase II and regulation of TFR2 expression by epigenetics.

3.6 | Tazemetostat targeting of EZH2 increases sorafenib sensitivity in vitro and in vivo

Given EZH2's observed role in mitigating sorafenib-induced ferroptosis in HCC cells, we hypothesized that utilizing EZH2 inhibitors could enhance sorafenib's therapeutic efficacy. The results demonstrated that the EZH2 inhibitor tazemetostat, in combination with sorafenib, synergistically decreased IC50 values (Figure 7A,B). Subcutaneous xenograft tumor analysis revealed that tazemetostat reduced tumor sizes and weights, with the combination of tazemetostat and sorafenib yielding smaller tumor volumes and weights compared with sorafenib alone (Figure 7C–E). Extensive tumor tissue necrosis induced by the tazemetostat and sorafenib combination and a significant decrease in Ki-67-positive cells were observed (Figure 7F–H). Immunohistochemical analysis indicated that tazemetostat reduced EZH2-positive cells and increased TFR2-positive cells. Moreover, the combination treatment group showed a further decrease in EZH2-positive cells and an increase in TFR2-positive cells compared with the sorafenib-alone group (Figure 7I–K). Tazemetostat increased MDA and iron levels concentration, with the combination group displaying higher levels compared with sorafenib alone (Figure 7L,M). These findings collectively suggest that tazemetostat upregulates TFR2 expression, increasing intracellular iron concentration, and, in synergy with sorafenib, induces ferroptosis, enhancing sorafenib's therapeutic effect on xenograft tumors.

FIGURE 5 EZH2 inhibits sorafenib-induced ferroptosis. (A) Analysis of the relationship between the expression of EZH2 and the sensitivity to chemotherapy drugs. (B) Sorafenib sensitivity detected by CCK-8 ($n=6$). (C) Colony formation ability detection ($n=3$). (D) EdU staining for the detection of the effect of HepG2 cell proliferation ($n=3$). (E) Detection of the effect of reactive oxygen species (ROS). (F) GSH/GSSG. (G) Malondialdehyde (MDA) levels and (H) mitochondrial membrane potential in HepG2 cells after EZH2 overexpression and exposure to sorafenib ($n=3$). Scale bar$=200\,\mu m$. (I) Representative images of mitochondrial morphology in HepG2 cells treated with sorafenib after overexpression of EZH2 detected by transmission electron microscope (TEM) ($n=3$). Scale bar$=1\,\mu m$ $^*p<0.05$; $^{**}p<0.01$.
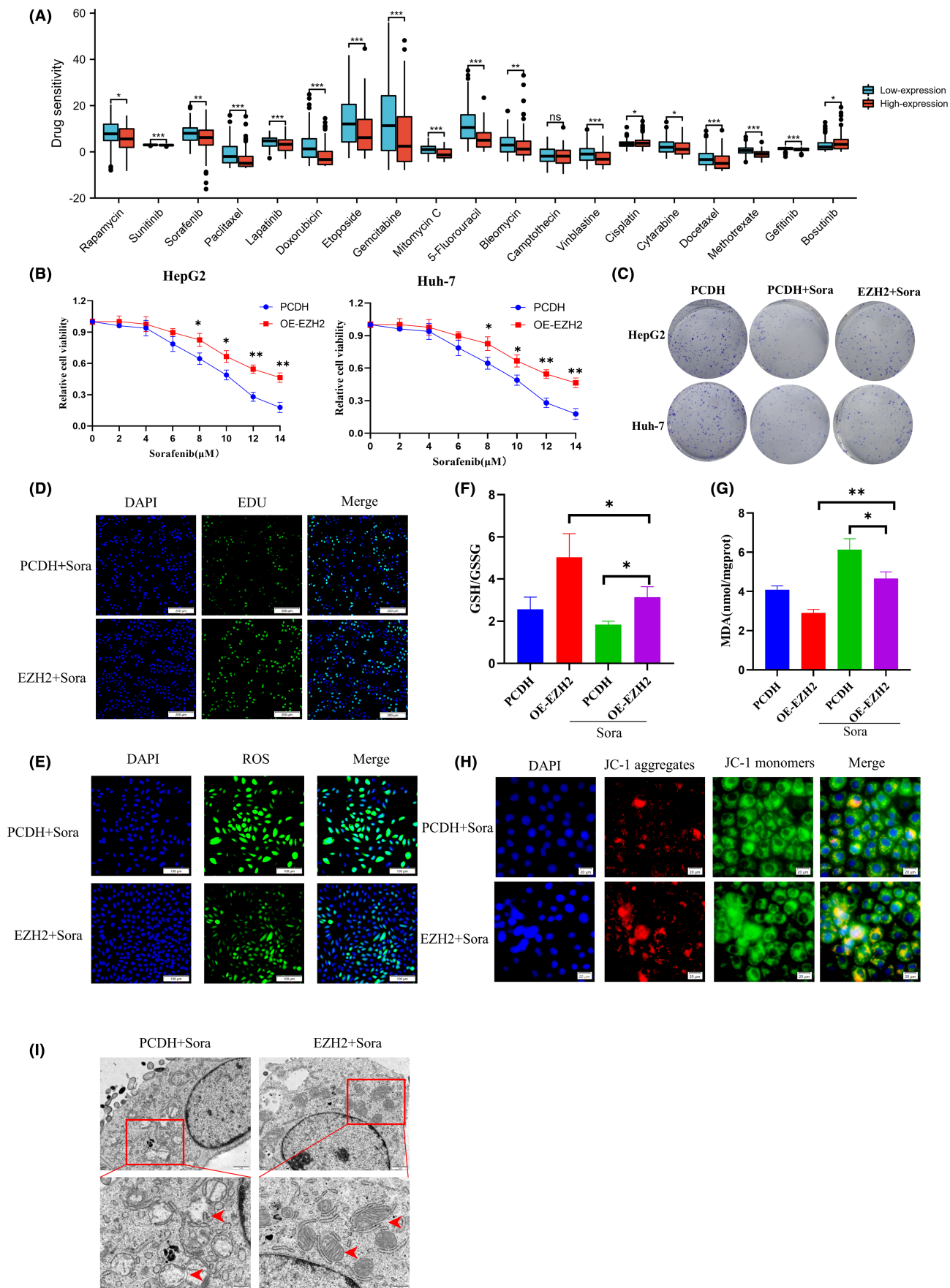
3.7 | Tazemetostat sensitizes the resistance of HCC cells to sorafenib

To investigate the role of tazemetostat combined with sorafenib in sorafenib-resistant HepG2 cells (HepG2-SR), we constructed HepG2-SR cells and detected the IC50 of sorafenib (Figure 8A). EZH2 expression in HepG2-SR cells was increased (Figure 8B, Figure S5A). Tazemetostat demonstrated the ability to suppress cell viability in HepG2-SR cells, with a synergistic effect observed when combined with sorafenib (Figure 8C). Tazemetostat combined with sorafenib reduced the expression of SLC7A11 and NRF2 and increase TFR2 proteins in HepG2-SR cells (Figure 8D, Figure S5B). In HepG2-SR cells, there was a decrease in the levels of ROS, Fe^{2+}, and MDA, accompanied by an increase in the levels of GSH/GSSH. Tazemetostat treatment led to an increase in ROS, Fe^{2+}, and MDA levels in HepG2-SR cells, while reducing GSH/GSSH levels (Figure 8E–H, Figure S5C). TEM imaging demonstrated that tazemetostat induced mitochondrial cristae damage in HepG2-SR cells, with the addition of sorafenib exacerbating this damage (Figure 8I). The above results indicate that tazemetostat enhances the susceptibility of HCC cells to sorafenib resistance.

4 | DISCUSSION

Primary liver cancer is the sixth most common cancer and the third leading cause of cancer-related deaths. Sorafenib is an important treatment for liver cancer patients who cannot have surgery, but resistance to the drug is a major issue. Sorafenib may induce a type of cell death called ferroptosis.[15] Nevertheless, during sorafenib resistance, ferroptosis occurrence decreases, revealing a tight connection between ferroptosis and sorafenib resistance. Hence, developing novel and effective therapeutic approaches to enhance sorafenib sensitivity remains crucial.

Elevated expression of EZH2 in HCC is correlated with an unfavorable prognosis and discovery of increased EZH2 expression in HepG2-SR cells. However, EZH2's involvement in ferroptosis in HCC has not been previously reported. This study demonstrates that overexpressing EZH2 in HCC cells increases the expression of the ferroptosis marker SLC7A11 and NRF2. Concurrently, EZH2 elevates NRF2 expression, thereby increasing GSH levels and reducing MDA and Fe^{2+} concentration. In summary, one of EZH2's mechanisms contributing to HCC's malignant progression involves inhibiting ferroptosis. Whether the presence of EZH2 can reduce the reactivity of HCC cells to sorafenib by hindering ferroptosis remains

to be determined. Our experiment validated that EZH2 can alleviated the decrease in GSH level, increase in ROS and MDA caused by sorafenib and avoid mitochondrial damage, ultimately reducing HCC sensitivity to sorafenib.

Interest in the role of iron in cellular biological processes, especially in tumor growth and proliferation, has significantly increased.[16] Recent research has unveiled a connection between drug resistance and iron metabolism, aiming to leverage this understanding to reverse drug resistance.[17] Moreover, epigenetic mechanisms such as DNA methylation, histone modification, and post-transcriptional modification have been found to regulate iron homeostasis. Elevated iron levels may heighten susceptibility to ferroptosis.[18] Various genes or proteins involved in iron homeostasis, encompassing import, export, and storage, have been proven to influence ferroptosis sensitivity.[11,17] In our study, EZH2 was observed to lead to a reduction in intracellular iron levels, rendering cells insensitive to ferroptosis. To identify genes associated with EZH2, iron metabolism, and ferroptosis driver genes, we utilized the TCGA database, GeneCards database, and FerrDB database, respectively. The Venn diagram facilitated the identification of common genes among the three databases. TFR2 exhibited the most negative correlation with EZH2, thereby establishing TFR2 as a potential candidate gene.

The main role of transferrin receptors (TFRs) is to bind to transferrin, facilitating the delivery of iron into cells. Two subtypes exist: TFR1 and TFR2.[19] TFR1 and TFR2 exhibit distinct expression patterns, with TFR1 found in various tissues and TFR2 primarily found in liver tissues.[20] Recent studies indicate that TFR2 expression is notably low in gastric cancer and indicates a poor prognosis.[21] TFR2 expression in glioma tissues negatively impacts patient prognosis, while overexpression enhances temozolomide efficacy by inducing ferroptosis in glioma cells.[22] However, the reduced presence of TFR2 in HCC tissue lacks a clear explanation from previous studies. Our research uncovered that overexpression of EZH2 leads to reduced TFR2 expression. EZH2 functions in epigenetic repression by catalyzing the methylation of histone H3 lysine 27 as its primary catalytic component.[23] We propose that EZH2 inhibits TFR2 expression through epigenetic regulation involving H3K27 me3. Our chromatin immunoprecipitation experiment supported this hypothesis, demonstrating that increased EZH2 levels in HCC cells elevate H3K27 me3 in the TFR2 promoter region while reducing H3K27ac. Overall, EZH2's modulation of histone H3K27 me3 levels in the TFR2 promoter region affects iron homeostasis in HCC, thereby regulating ferroptosis.

EZH2 is a crucial gene that drives cancer's malignant progression, making the development of EZH2 inhibitors imperative.

FIGURE 6 EZH2 inhibits the expression of TFR2 by promoting H3K27 trimethylation of the TRF2 promoter region. (A) A Venn diagram showing overlap genes. (B) Correlation between EZH2 and overlap genes expression. (C) Expression of TFR2 in tumor and normal tissues in TCGA database ($n=271$). (D) Immunohistochemical staining (IHC) detection of EZH2 expression in eight pairs of hepatocellular carcinoma (HCC) tissues from patients ($n=8$). (E, F) PCR and Western blot detection of the effect of EZH2 overexpression on TFR2 expression ($n=3$). (G, H) PCR and Western blot detection of the effect of EZH2 knockdown on TFR2 expression ($n=3$). (I) ChIP detection of H3K27me3 (J), H3K27ac (K), and RNA polymerase II in the TFR2 promoter region ($n=3$). *$p<0.05$; **$p<0.01$; ***$p<0.001$.
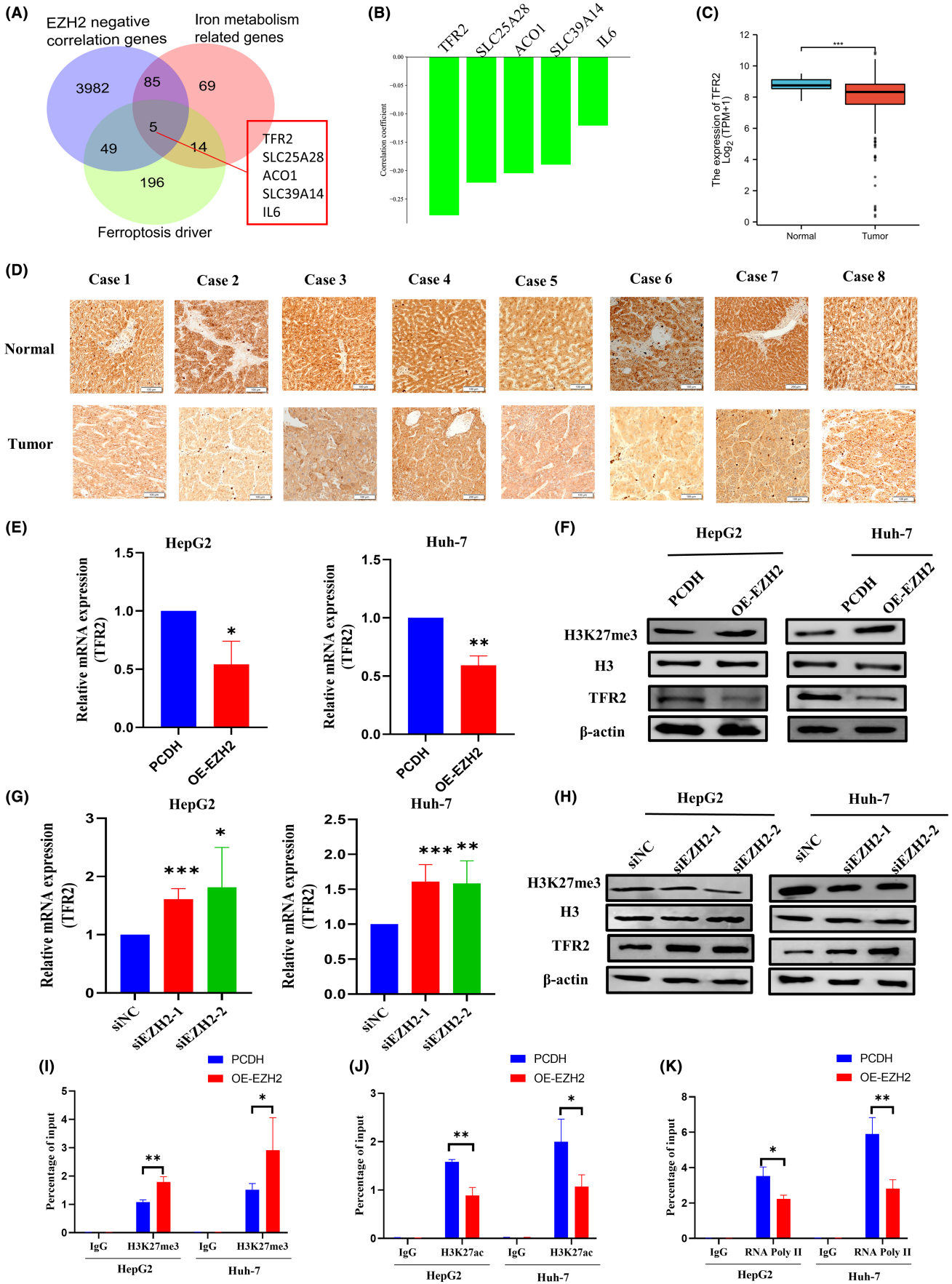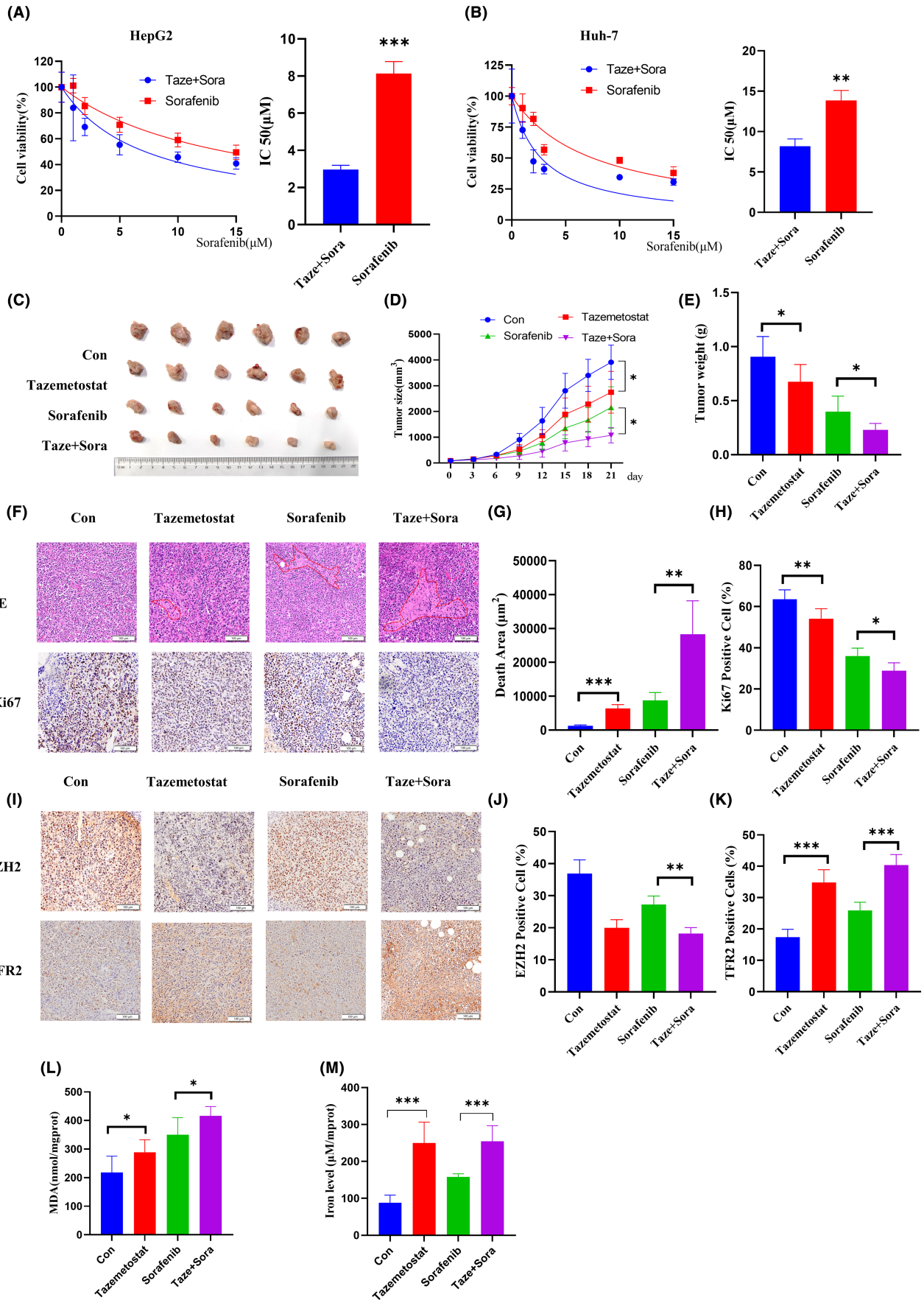
FIGURE 7 Tazemetostat targeting of EZH2 increases sorafenib sensitivity in vitro and in vivo. (A, B) HepG2 and Huh-7 cells were treated with tazemetostat and different concentrations of sorafenib, and the IC_{50} of sorafenib was calculated ($n=6$). (C). Tumor images from each treatment group ($n=6$). (D) Volume of the subcutaneous tumors ($n=6$). (E) Weight of the subcutaneous tumors ($n=6$). (F–H) Representative H&E staining image. Area of death and Ki-67-positive cell ratio ($n=6$). Scale bar $=100\,\mu m$. (I–K) Representative immunohistochemical staining (IHC) image of EZH2 and TFR2 ($n=6$). Scale bar $=100\,\mu m$. (L) Concentration of malondialdehyde (MDA). (M) Iron concentration in tumors of different treatment groups ($n=6$). $*p<0.05$; $**p<0.01$; $***p<0.001$.
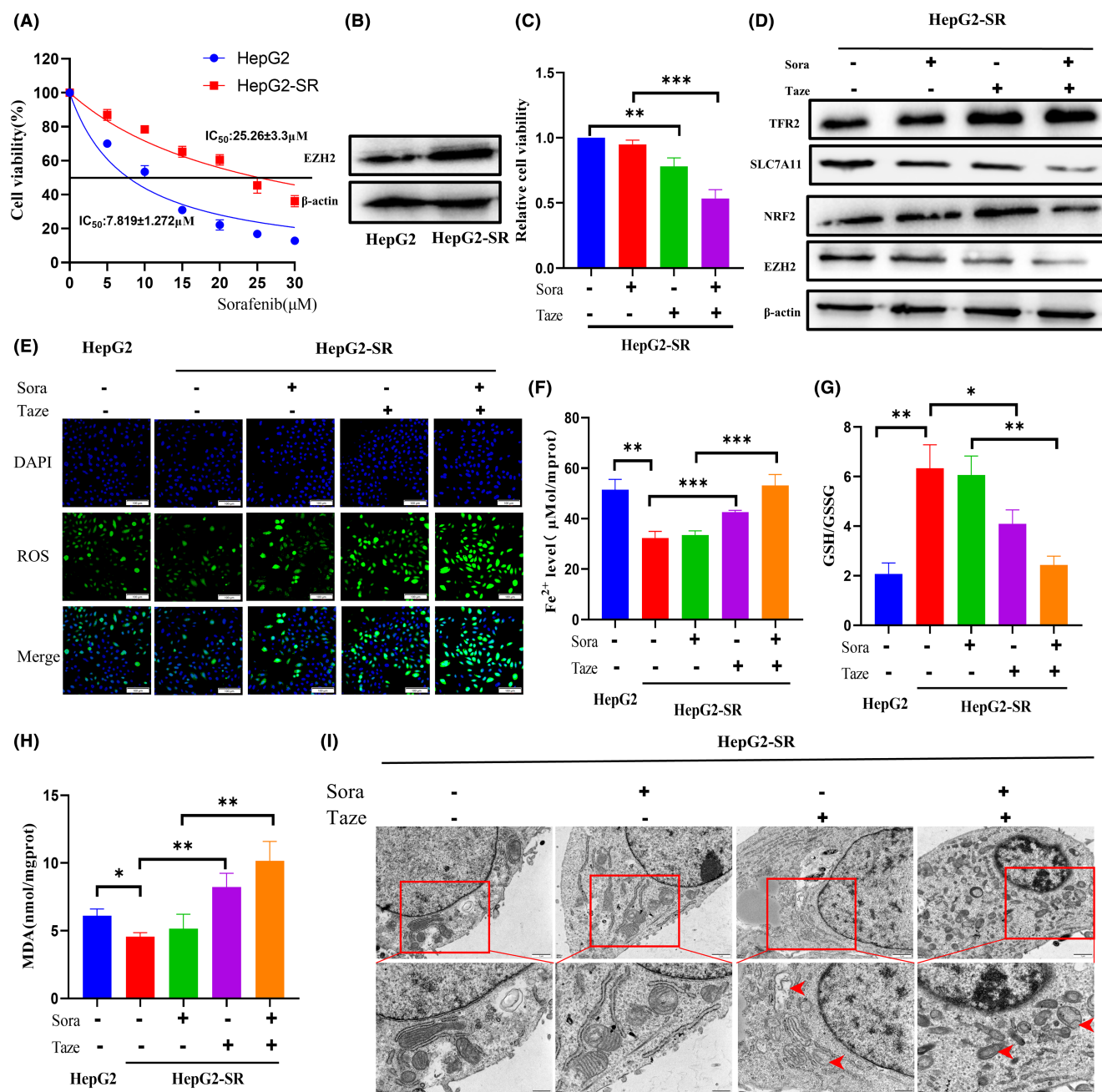

FIGURE 8 Tazemetostat sensitizes the resistance of hepatocellular carcinoma cells to sorafenib. (A) The sorafenib IC50 values of HepG2 and HepG2-SR cells ($n=3$). (B) Protein expression of EZH2 in HepG2 and HepG2-SR cells ($n=3$). (C) CCK-8 detection of the viability of tazemetostat combined with sorafenib on HepG2-SR cells ($n=3$). (D) Western blot detection of tazemetostat combined with sorafenib on ferroptosis-related protein in HepG2-SR cells ($n=3$). (E) Reactive oxygen species (ROS), (F) Fe^{2+}, (G) GSH/GSSG, and (H) Malondialdehyde (MDA) levels in HepG2-SR cells treated with tazemetostat combined with sorafenib ($n=3$). (I) Representative transmission electron microscope (TEM) images of mitochondrial morphology in HepG2-SR cells treated with tazemetostat combined with sorafenib ($n=3$) Scale bar $=1\,\mu m$. $*p<0.05$; $**p<0.01$; $***p<0.001$.
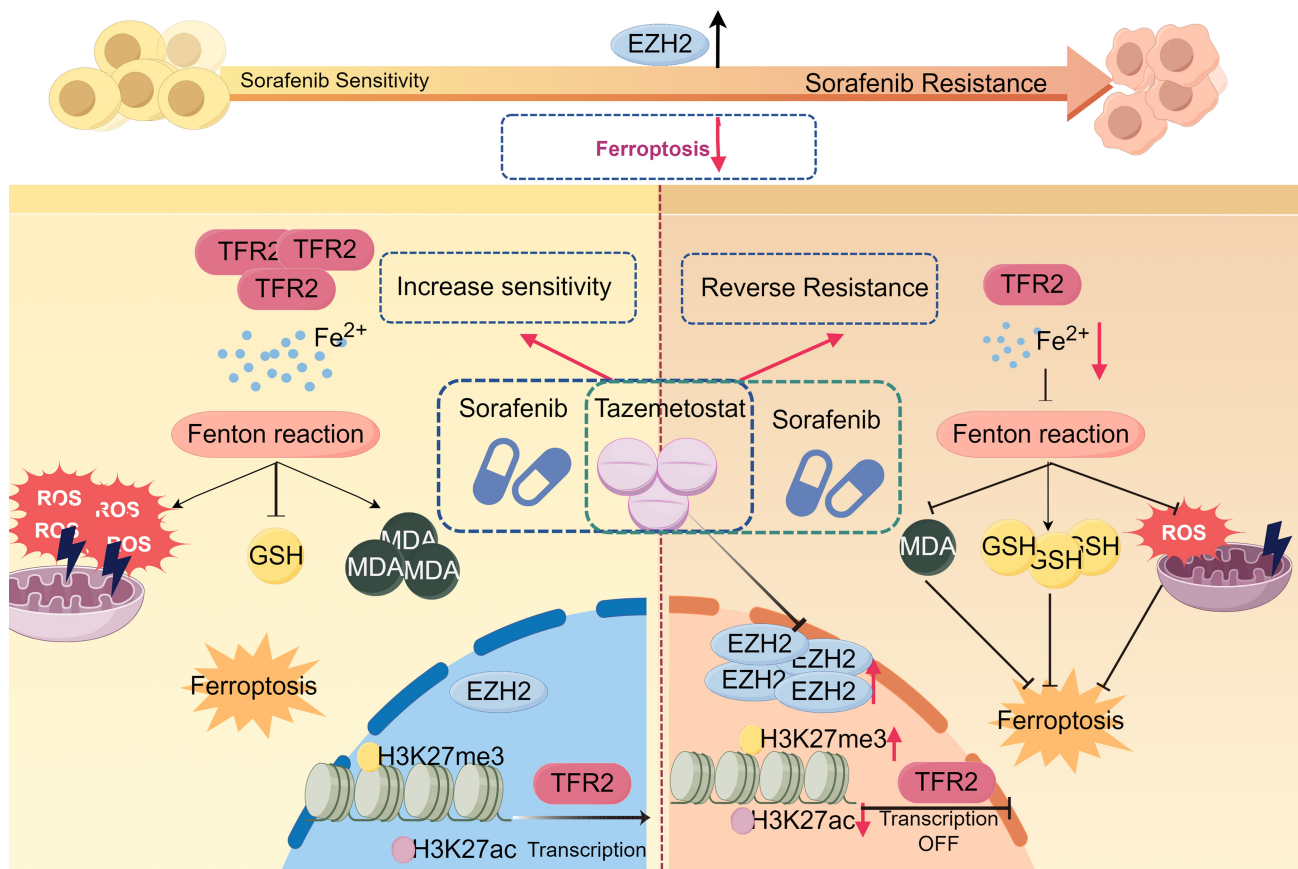
FIGURE 9 Schematic diagram showing that EZH2 inhibits ferroptosis and tazemetostat increases sorafenib sensitivity. EZH2, enhancer of zeste 2 polycomb repressive complex 2 subunit; MDA, malondialdehyde; ROS, reactive oxygen species; TFR2, transferrin receptor 2.

Consequently, these inhibitors have shown promise in cancer treatment. Tazemetostat (EPZ-6438), GSK126, and other inhibitors have been developed. Currently, only tazemetostat (EPZ-6438) has FDA approval for treating epithelioid sarcoma and follicular lymphoma.[24,25] However, the potential of tazemetostat as an EZH2 inhibitor in HCC and its mechanism to enhance sorafenib sensitivity remains unexplored. In vivo experiments revealed that tazemetostat, in conjunction with sorafenib, effectively inhibits tumor tissue growth and synergistically suppresses EZH2 and Ki67 expression in tumors. In HepG2-SR cells, it could sensitize the resistance of HCC cells to sorafenib. Specifically, it inhibits EZH2, downregulates SLC7A11 and NRF2, and reversing the silencing of TFR2 gene, thereby elevating iron accumulation and inducing the Fenton reaction to facilitate ferroptosis. These findings offer practical insights into using tazemetostat and sorafenib clinically for HCC treatment.

In summary, our study found that EZH2 was highly expressed in HCC, and its high expression was correlated with poor patient prognosis. The mechanisms were the epigenetic regulation of TFR2 expression through H3K27me3 and inhibition of ferroptosis. The EZH2 inhibitor tazemetostat synergized with sorafenib and had superior synergistic effects in anticancer therapy in vitro and in vivo (Figure 9). Tazemetostat could enhance sorafenib treatment in HCC and sensitize the resistance of HCC cells to sorafenib.

AUTHOR CONTRIBUTIONS

Yongwei Lai: Conceptualization; methodology; validation. **Xu Han:** Software. **Bo Xie:** Validation. **Yan Xu:** Investigation. **Zhengyi Yang:** Formal analysis. **Didi Wang:** Software. **Wei Li:** Methodology. **Yaohong Xie:** Software; validation. **Wenqi Song:** Formal analysis. **Xiaohong Zhang:** Investigation. **Jia Qi Xia:** Conceptualization; funding acquisition. **Pengxia Zhang:** Conceptualization; funding acquisition; project administration.

CONFLICT OF INTEREST STATEMENT

The authors have no conflict of interest.

ETHICS STATEMENTS

Approval of the research protocol by an Institutional Reviewer Board: N/A.

Informed Consent: An informed consent form was signed by patients in accordance with the Declaration of Helsinki, and the study was approved by the Ethics Committee of Jiamusi University.

Registry and the Registration No. of the study: N/A.

Animal studies: The animal study received approval from the Ethics Committee of Jiamusi University.

ORCID

Jia Qi Xia https://orcid.org/0000-0002-3781-7378
Pengxia Zhang https://orcid.org/0000-0002-6114-1080

REFERENCES

1. Bruix J, Reig M, Sherman M. Evidence-based diagnosis, staging, and treatment of patients with hepatocellular carcinoma. *Gastroenterology*. 2016;150:835-853.
2. Cheng AL, Kang YK, Chen Z, et al. Efficacy and safety of sorafenib in patients in the Asia-Pacific region with advanced hepatocellular carcinoma: a phase III randomised, double-blind, placebo-controlled trial. *Lancet Oncol*. 2009;10:25-34.
3. Vogel A, Meyer T, Sapisochin G, Salem R, Saborowski A. Hepatocellular carcinoma. *Lancet*. 2022;400:1345-1362.
4. Wang S, Zhu Y, He H, et al. Sorafenib suppresses growth and survival of hepatoma cells by accelerating degradation of enhancer of zeste homolog 2. *Cancer Sci*. 2013;104:750-759.
5. Wu PC, Kao LS. Calcium regulation in mouse mesencephalic neurons-differential roles of Na(+)/Ca(2+) exchanger, mitochondria and endoplasmic reticulum. *Cell Calcium*. 2016;59:299-311.
6. Louandre C, Marcq I, Bouhlal H, et al. The retinoblastoma (Rb) protein regulates ferroptosis induced by sorafenib in human hepatocellular carcinoma cells. *Cancer Lett*. 2015;356:971-977.
7. Guo L, Hu C, Yao M, Han G. Mechanism of sorafenib resistance associated with ferroptosis in HCC. *Front Pharmacol*. 2023;14:1207496.
8. Li Z, Hou P, Fan D, et al. The degradation of EZH2 mediated by lncRNA ANCR attenuated the invasion and metastasis of breast cancer. *Cell Death Differ*. 2017;24:59-71.
9. Chan AL, La HM, Legrand J, et al. Germline Stem cell activity is sustained by SALL4-dependent silencing of distinct tumor suppressor genes. *Stem Cell Rep*. 2017;9:956-971.
10. Duan R, Du W, Guo W. EZH2: a novel target for cancer treatment. *J Hematol Oncol*. 2020;13:104.
11. Hassannia B, Vandenabeele P, Vanden BT. Targeting ferroptosis to iron out cancer. *Cancer Cell*. 2019;35:830-849.
12. Hino K, Yanatori I, Hara Y, Nishina S. Iron and liver cancer: an inseparable connection. *FEBS J*. 2022;289:7810-7829.
13. Nie J, Lin B, Zhou M, Wu L, Zheng T. Role of ferroptosis in hepatocellular carcinoma. *J Cancer Res Clin Oncol*. 2018;144:2329-2337.
14. Farida B, Ibrahim KG, Abubakar B, et al. Iron deficiency and its epigenetic effects on iron homeostasis. *J Trace Elem Med Biol*. 2023;78:127203.
15. Louandre C, Ezzoukhry Z, Godin C, et al. Iron-dependent cell death of hepatocellular carcinoma cells exposed to sorafenib. *Int J Cancer*. 2013;133:1732-1742.
16. Torti SV, Torti FM. Iron and cancer: 2020 vision. *Cancer Res*. 2020;80:5435-5448.
17. Kazan HH, Urfali-Mamatoglu C, Gunduz U. Iron metabolism and drug resistance in cancer. *Biometals*. 2017;30:629-641.
18. Lee J, Roh JL. Epigenetic modulation of ferroptosis in cancer: identifying epigenetic targets for novel anticancer therapy. *Cell Oncol (Dordr)*. 2023;46:1605-1623.
19. Yang Y, Zuo S, Li L, et al. Iron-doxorubicin prodrug loaded liposome nanogenerator programs multimodal ferroptosis for efficient cancer therapy. *Asian J Pharm sci*. 2021;16:784-793.
20. Fleming RE, Migas MC, Holden CC, et al. Transferrin receptor 2: continued expression in mouse liver in the face of iron overload and in hereditary hemochromatosis. *Proc Natl Acad Sci USA*. 2000;97:2214-2219.
21. Zhao QF, Ji J, Cai Q, et al. Low expression of transferrin receptor 2 predict poor prognosis in gastric cancer patients. *Kaohsiung J Med Sci*. 2020;36:1014-1020.
22. Tong S, Hong Y, Xu Y, et al. TFR2 regulates ferroptosis and enhances temozolomide chemo-sensitization in gliomas. *Exp Cell Res*. 2023;424:113474.
23. Gao SB, Zheng QF, Xu B, et al. EZH2 represses target genes through H3K27-dependent and H3K27-independent mechanisms in hepatocellular carcinoma. *Mol Cancer Res*. 2014;12:1388-1397.
24. Knutson SK, Kawano S, Minoshima Y, et al. Selective inhibition of EZH2 by EPZ-6438 leads to potent antitumor activity in EZH2-mutant non-Hodgkin lymphoma. *Mol Cancer Ther*. 2014;13:842-854.
25. Genta S, Pirosa MC, Stathis A. BET and EZH2 inhibitors: novel approaches for targeting cancer. *Curr Oncol Rep*. 2019;21:13.

SUPPORTING INFORMATION

Additional supporting information can be found online in the Supporting Information section at the end of this article.